Estimating the effect of cold forming and post processing on fatigue of high strength steels under component-related loading conditions

Engineering Failure Analysis 184 (2026) 110368

Contents lists available at ScienceDirect

Engineering Failure Analysis

journal homepage: www.elsevier.com/locate/engfailanal

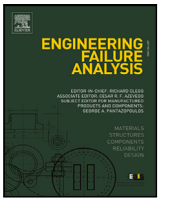

Estimating the effect of cold forming and post processing on fatigue of high strength steels under component-related loading conditions

David Gustafsson [a], Davide Ronco [b], Giorgio Gallio [b], Erik Olsson [a,*]

[a] Luleå University of Technology, Department of Engineering Sciences and Mathematics, Division of Solid Mechanics, Luleå, SE-971 87, Sweden
[b] MW Italia srl, Via Pavia 72, Rivoli (TO), 10098, Italy

ARTICLE INFO

Keywords:
High cycle fatigue
Residual stresses
High strength steel
Bending
Cold forming

ABSTRACT

Stamping and shot peening of chassis components such as wheels and cross beams introduce residual stresses that affect the fatigue life. The tensile residual stresses from stamping are often found in the most critical areas for fatigue. These areas are commonly subject to bending stress states while smooth material fatigue data for steel sheets more commonly is obtained by uniaxial testing. Both the sensitivity to residual stresses and change in load condition are material dependent posing a challenge in fatigue life estimation of formed and shot-peened specimens. This paper aims to provide a convenient tool for high cycle fatigue life estimations in these conditions solely dependent on uniaxial tensile properties without parameter fitting. The underlying causes for the material dependency is discussed and reflected in the methodology. Uniaxial fatigue testing and fatigue testing of formed specimens with and without subsequent shot peening are performed for validation.

1. Introduction

Cold stamping is a common process in the production of automotive components, especially chassis components [1] and steel wheels [2]. Steel wheels are composed of two main units [3], the stamped disc and the roll-formed [4] rim, as shown in Fig. 1. Some regions of the disc are particularly stressed and susceptible to fatigue [5]. Thickness reduction, strain hardening or softening, and residual stresses have been mentioned as important factors contributing to the different fatigue strength in formed areas as compared to the base material fatigue strength [6–8]. In addition, for some steels, the paint baking cycle can have a negative effect on fatigue life due to carbon nitrides forming at the grain boundaries [9], and pre-stresses from the wheel assembly might be present [10].

It is well known that the stamping process often induces significant residual stresses that for some loading conditions are detrimental for the fatigue life of the component. In [9] it was shown that the fatigue life of a wheel disc had a closer correlation with the residual stresses than with the hardness. It was stated that bending was the predominant loading mode in fatigue of wheel discs. Discs produced of a dual phase steel of grade 600 were studied and the residual stresses were measured close to the cup radius on disc components after complete production. Tensile residual stresses of a magnitude around 70% of the yield strength were found. The fatigue tests were performed at load ratio $R = -1$.

The fatigue life reduction due to tensile residual stresses could also increase with material strength [11,12], posing a challenge in the constant pursuit of grams to reduce fuel consumption. On the other hand, the effect of strain hardening on fatigue can decrease as the material strength increases [13]. Hence, a life estimation model able to account for the residual stresses from forming seems tempting. It could be used to increase the understanding of why some materials perform better than others in fatigue after forming

* Corresponding author.
E-mail address: erik.1.olsson@ltu.se (E. Olsson).

https://doi.org/10.1016/j.engfailanal.2025.110368
Received 10 September 2025; Received in revised form 6 November 2025; Accepted 18 November 2025
Available online 19 November 2025

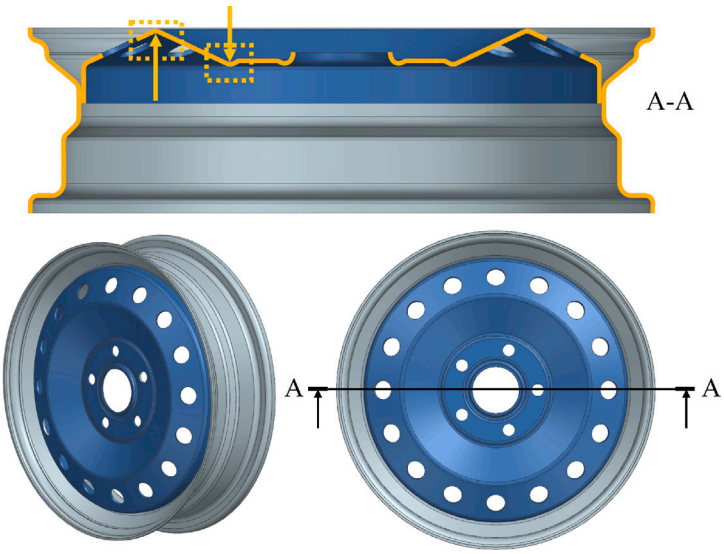

Fig. 1. Steel wheel composed by a disc (blue) and a rim (gray). The arrows point out critical locations for fatigue crack initiation.

and give an estimation to when post processing is necessary to achieve satisfactory fatigue performance. This is especially important in development of safety component such as the wheel, where the durability must be secured [6].

In [7] a local fatigue life estimation method was proposed, accounting for stretching and bending induced plasticity. The incorporation of residual stresses was left as future work. Analytical expressions were established to calculate the local stresses and strains in the fatigue-sensitive areas. The material orthotropy due to the rolling direction was neglected and the method was considered valid for small curvatures where the local strain was lower than 10% in bending. The calculated von Mises equivalent plastic strain ε_p was translated into an increase of the base material endurance limit $\sigma_{\infty 0}$ using

$$\frac{\sigma_\infty}{\sigma_{\infty 0}} = 1 + A\varepsilon_p, \tag{1}$$

where σ_∞ is the new fatigue limit and A is a material and load case dependent parameter in the range of 1 to 4 for most cases, meaning that the fatigue limit would increase at least as many percent as the local plastic strain. This magnitude of endurance limit increase was confirmed for DP590 in [14] where 10% uniaxial prestraining resulted in a fatigue strength increase of 11%. For notched specimens the effect of prestraining is small, which could be explained by a corresponding increase in stress concentration as the material fatigue strength increases [1].

One of the most critical fatigue tests for wheels is the dynamic cornering test [15]. The stress state during this test was simulated in [15] and it was found that the fatigue cracks were mainly caused by normal stresses in the radial direction of the wheel.

In [6] a multi-step stamping process of a wheel disc was simulated, and the resulting thickness change and effective strain were used for fatigue life estimation. It was stated that the residual stress could have a great influence but due to uncertainties in the residual stress levels and relaxation rates, these were disregarded.

To summarize the studies mentioned, bending often seems to be an important load case for fatigue on component level and the residual stresses seems to affect the high cycle fatigue life.

A new specimen design was proposed in [16] to explore process effects on bending fatigue. The studied material was hot rolled S500MC steel sheets of thickness 12 mm. To maintain plane strain bending conditions the specimen width was set to 68 mm. A load ratio of $R = 0.1$ was used for the fatigue testing. The fatigue stress range was taken as the longitudinal stress component range in FEM (Finite Element Method) simulations of the load case. It was stated that 16 elements through the thickness were needed to safely reach convergence of the surface stress. In the forming simulations a friction coefficient of 0.05 was used. A decreasing magnitude of residual stress was found as the ratio between radius and thickness increased.

In [8], reverse engineering was used to extract stamping process results in terms of plastic deformations and thickness changes starting from the final geometry and material data. This information was then used for fatigue life estimation. The residual stresses were disregarded with the motivation that the cyclic stress amplitude in the critical locations exceeded the yield strength of the studied materials.

Several steps of the wheel production process were simulated in [10] using a FEM model composed of shell elements, and the results were used for fatigue life estimation. The work was focusing on stresses arising from the wheel assembly. The stamping process effects such as thinning, prestraining and residual stresses were not considered but were left as future work.

In [4] fatigue of the rims were studied through rim-rolling simulations and subsequent transfer of residual stress information to a fatigue life estimation model. By superimposing the residual stress field to the applied stresses, a better agreement between fatigue life estimations and experiments was obtained.

The works mentioned above shows that the effect of forming induced residual stresses is often mentioned as a possible source for fatigue life reduction of steel wheels, but that life estimation methods to conveniently account for this are lacking. This effect is also material dependent. Concerning the stamped discs in particular, the effect of residual stresses on fatigue, including cyclic stress relaxation and different hardening behavior, has not, to the best of the authors knowledge, been thoroughly investigated.

This work aims to use a simplified specimen geometry that captures the forming induced effects and the major parts of the in-service loading conditions to develop and experimentally validate a fatigue life estimation procedure. The method could for example be used in early development phases to rank and compare design shapes and materials in terms of fatigue strength.

To reach this goal stamped specimens of three different high strength steels were produced and tested in high cycle fatigue (HCF). FEM simulations of the clamping process were performed to evaluate the mean stresses due to different springback from forming. The residual stresses in the critical zone where fatigue cracks initiated were measured and conveniently incorporated in a fatigue life estimation model. The base *S-N* curves used as starting points for the estimated reduced curves were obtained from uniaxial testing and hence a conversion from uniaxial fatigue to bending fatigue was implemented. In addition, the effect of shot peening was studied to explore the possibilities of fatigue enhancing post processes.

2. Theory

In [17] a method for HCF life estimation of punched and trimmed specimens subject to uniaxial loading was presented. This method was later used in [18] for specimens subject to out-of-plane bending. Neglecting the surface roughness treatment, necessary for cut edges, the reduced fatigue life $\sigma_a'(N)$ is stated to be estimated by

$$\sigma_a' = K_{m\sigma}\left(\frac{1}{K_t}\right)^{h_t}\sigma_{a-1} \tag{2}$$

where σ_{a-1} is the *S-N* curve for as-rolled specimens with polished edges at $R=-1$ obtained through uniaxial testing, $K_{m\sigma}$ accounts for mean stresses including residual stresses, and K_t is an elastic stress concentration factor. The exponent h_t increases the impact of elastic stress concentration as the number of cycles increases, and is given by

$$h_t = \frac{1}{6}\log_{10}(N) \tag{3}$$

with limits set so that it obtains a value of 0 for all values below zero and 1 for all values above 1.

The expression for $K_{m\sigma}$ is, following [18] based on the Gerber parabola (Q=2) for positive mean stresses and the Goodman's model (Q=1) for compressive stresses so that [19–21]

$$K_{m\sigma} = 1 - \left(\frac{\sigma_m + \sigma_{res}}{\sigma_{uts}}\right)^{Q} \tag{4}$$

where σ_{uts} is the uniaxial ultimate tensile strength, σ_m is the nominal mean stress of the as-rolled specimens. The stabilized residual stress, after cyclic relaxation, σ_{res} is estimated by [18]

$$\sigma_{res} = \begin{cases} \sigma_y - \sigma_{max}, & \text{if } \sigma_{res}^0 > \sigma_y - \sigma_{max} \\ -0.48\sigma_y + 0.33\sigma_{max}, & \text{if } \sigma_{res}^0 < -0.48\sigma_y + 0.33\sigma_{max} \\ \sigma_{res}^0, & \text{if } -0.48\sigma_y + 0.33\sigma_{max} \le \sigma_{res}^0 \le \sigma_y - \sigma_{max}, \end{cases} \tag{5}$$

where σ_y is the monotonic yield stress at 0.2% plastic strain, σ_{res}^0 is the initial surface residual stresses in the loading direction in the region of crack initiation, and σ_{max} is the nominal maximum stress, see Fig. 2. The implementation of the relaxation criteria based on the nominal maximum stress, as done in [17,18] introduces an inconsistency with the theory as the relaxation is calculated, not on the actual stress level of testing, but at the nominal stress level before reduction due to residual stress. However, it has demonstrated capabilities in modeling the HCF reduced fatigue life of specimens containing both compressive and tensile residual stresses [17,18].

In [17,18] a constant load ratio was used. In this work on the other hand a state of constant mean stress σ_m due to clamping stresses is assumed, further described later. Hence, the maximum nominal stress can be calculated by

$$\sigma_{max} = \sigma_m + \sigma_{a-1}\left[1 - \left(\frac{\sigma_m}{\sigma_{uts}}\right)^{Q}\right]. \tag{6}$$

3. Material and methods

3.1. Materials

The materials used in the study were hot rolled CP800SF, DP600, and DP780, where DP600 represents the current state of the art in steel wheel production [1,22].

Tensile properties are required information for utilization of the fatigue life estimation method in [17]. No tensile tests were performed in this work, instead, the information for HR CP800SF in [23] and the material data from MW Italia S.r.l. were relied upon. The mechanical properties of the studied materials are presented in Table 1. The nominal thicknesses used for HR DP780 and HR DP600 were 3.0 and 3.5 mm, respectively. In the case of HR CP800SF, the bent specimens were produced in another thickness

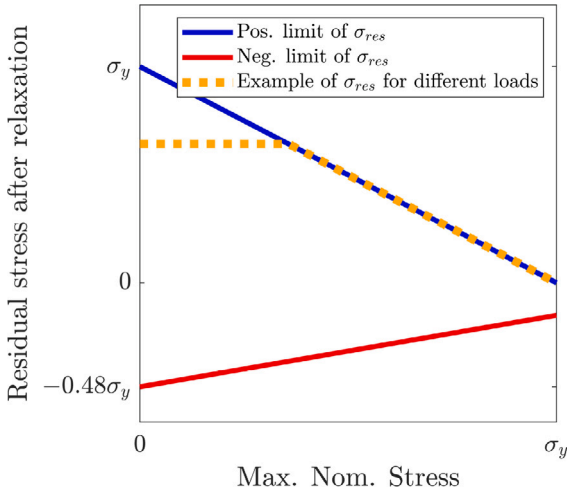

Fig. 2. Cyclic stress relaxation criterion.
Source: From [18].

Table 1
Uniaxial tensile properties of the studied materials. Yield stress σ_y at 0.2% plastic strain and tensile strength σ_{uts}. Properties for HR CP800SF are obtained from [23] and the properties for the other materials are supplied by MW Italia S.r.l.

Mtrl.	σ_y [MPa]	σ_{uts} [MPa]
HR CP800SF	778	835
HR DP600	385	590
HR DP780	531	812

(3.7 mm), as compared to the uniaxial specimens (3.4 mm). Equal material properties were assumed for the different thicknesses. This assumption was justified mainly by the fact that the sheets were produced by hot rolling where the metal is formed above its recrystallization temperature [24]. In cold rolling, on the other hand, work hardening during the thickness reduction is expected to influence the mechanical properties. The different CP steel sheets used in this study were also the same grade produced by the same company. In [25], thin hot-rolled sheets were shown to be relatively unaffected by sheet thickness in terms of microstructure and texture, which in turn govern mechanical properties. In [26] hot rolled DP590 steel showed a decrease of 1.1% in yield strength when the thickness was increased from 3 to 11 mm. The corresponding decrease in tensile strength was 7.9%. In this work the thickness difference was 0.3 mm. Assuming similar properties might still introduce some uncertainty to the results, also due to the fact that the material can come from different production batches.

3.2. Manufacturing of bent and straight fatigue specimens

To reproduce the loading conditions and forming history found in some of the critical locations of the wheel without requiring full wheel component testing, a specimen geometry and production methodology were proposed in [27]. The specimens, see Fig. 3 used in this work were produced according to [27] except for the optional hole since the aim only was to evaluate the influence of the stamping process on the HCF strength. The punching process effects on fatigue were studied in previous works [17,23]. Some of the specimens were shot peened after forming.

Due to different material properties, sheet thicknesses and post processes, the geometries after forming exhibited differences between the studied materials. To account for this at least three specimens of each material were measured along the center line (the dashed orange line in Fig. 3) of the specimen using a coordinate-measuring machine (CMM). The average of the measurements (A-F) for each material are presented in Table 2. The parameters C and R1 were measured on both sides of the symmetry line and then averaged.

The geometry of the uniaxial fatigue specimens is presented in Fig. 4. The edges of the specimen are polished, and the top and bottom surfaces are in as-rolled condition.

Table 2
CMM geometry measurement results after forming, and after forming followed by shot peening.

Mtrl.	A [mm]	B [mm]	C [°]	R1 [mm]	E [mm]	R2 [mm]
HR CP800SF	203.5	87.5	1.0	18.9	38.8	12.0
HR CP800SF (SP)	203.9	88.0	0.8	19.2	38.4	12.3
HR DP600	202.3	85.1	0.0	18.3	38.9	11.7
HR DP600 (SP)	203.8	88.1	−0.4	20.6	38.2	12.1
HR DP780	207.1	87.4	0.3	18.5	35.0	10.8
HR DP780 (SP)	207.9	87.8	−0.4	18.8	34.0	11.8

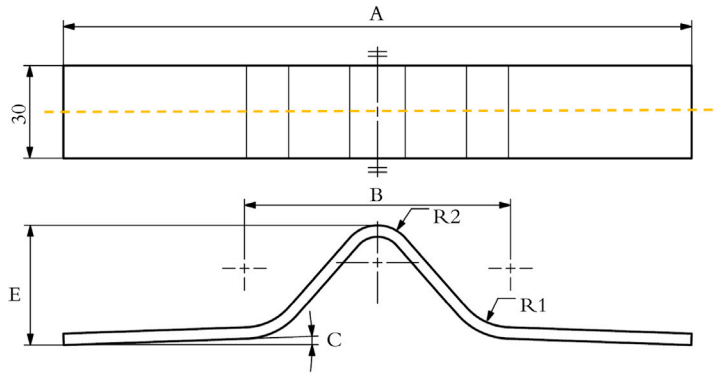

Fig. 3. Geometry of the bent fatigue specimens. [mm].

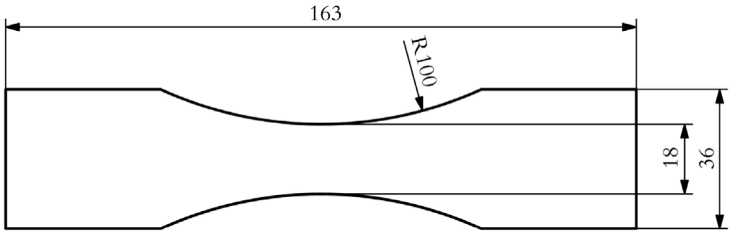

Fig. 4. Geometry of the straight fatigue specimen. [mm].

3.3. Clamping simulations to obtain mean stresses

Implicit FEM simulations of the clamping process used in the fatigue testing were conducted to obtain the correct mean stress in the loading direction for each material with and without shot peening. The simulation setup, using a quarter of the specimen and symmetry conditions, is presented in Fig. 5. Solid eight node elements were used with a width of 0.183 mm and a height of the sheet thickness divided by 20. 40 mm of the specimen was clamped on each side. A linear elastic material model was used with an elastic modulus of 200 GPa and Poisson's ratio 0.3.

3.4. Simulation of axial loading to calculate nominal stress

The simulated resulting geometries in clamped condition were used for implicit FEM simulations of applied axial displacement of the nodes in the clamped region. The displacement was set to 0.3 mm in the Y-direction. The moment around the X-axis M_x close to the center of the specimen, and the force in the Y-direction, were measured. The nominal maximum stress amplitude from loading in the bent radius can be calculated according to

$$\sigma_a = \frac{M_x}{I_x}\frac{t}{2} + \frac{F_y}{Wt}, \tag{7}$$

where W and t are the width and thickness of the specimens, respectively, F_y is the force along the Y-direction, and I_x is the moment of inertia of the rectangular cross section calculated as

$$I_x = \frac{Wt^3}{12}. \tag{8}$$

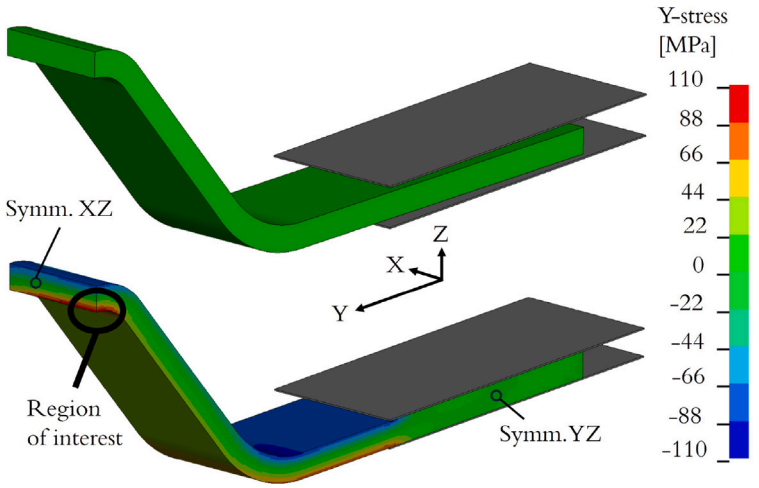

Fig. 5. Example (3.7 mm HR CP800SF) FEM simulation setup of clamping for subsequent fatigue testing.

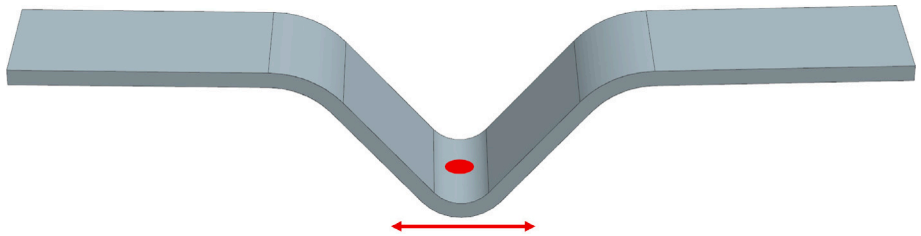

Fig. 6. XRD residual stress measurement position.

Table 3
Factor to calculate moment from test force in the section of interest, and elastic stress concentration factors for each configuration.

Mtrl.	k [Nm/N]	K_t [-]
HR CP800SF	21.58	1.17
HR CP800SF (SP)	21.46	1.17
HR DP600	22.68	1.17
HR DP600 (SP)	22.52	1.16
HR DP780	20.42	1.16
HR DP780 (SP)	20.34	1.14

With these simulations, assuming a linear relationship between the applied force in fatigue testing and the moment in the radius, a conversion factor k between the applied force in testing and the resulting moment could be established for each configuration. Hence, the nominal maximum stress amplitude for each applied load in the experiment could be calculated according to

$$\sigma_a = \frac{kF_y}{I_x}\frac{t}{2} + \frac{F_y}{Wt}. \tag{9}$$

By comparing the simulated stress in the center of the radius to the nominally calculated stress, an elastic stress concentration factor K_t could also be established for each configuration. These values and the conversion factors are presented in Table 3.

3.5. Residual stress measurements

The residual stresses in the longitudinal direction of the specimens were measured on the inside of the bent radius in the center as shown in Fig. 6 using X-ray diffraction (XRD). Measurements were performed on at least six specimens per material and post processing option. Half of the specimens were cut transverse to the rolling direction and half along the rolling direction.

Table 4
Basquin parameters ($R = -1$) for the studied materials for specimens with polished edges. The values for HR CP800SF are obtained from [17].

Material	C [MPa]	m [-]
HR CP800SF	2004.80	7.885
HR DP600	637.716	15.56
HR DP780	1057.31	11.57

3.6. Fatigue testing of uniaxial and bent specimens

Uniaxial fatigue testing of flat specimens according to SEP1240 was conducted to create the base material *S-N* curves. The fatigue tests presented in Tables A.1–A.3, including the tests of the bent specimens, were set to terminate if the total displacement of the grips exceeded 2 mm. The *S-N* curves were created by fitting a Basquin curve to the experimental data, creating a 50% failure probability curve on the form [28]

$$\sigma_a = CN^{-1/m}, \tag{10}$$

where N is the number of cycles to failure of the specimen. C and m are used as calibration parameters in this work.

The fitted Basquin parameters are presented in Table 4. The parameters for HR CP800SF are obtained from [17]. A few fatigue tests using this material were conducted confirming the validity of the curve. These tests also verifies the failure criterion based of grip displacement instead of total fracture used in [17].

3.7. Extension of life estimation method to enable different loading modes

In [17] reduced fatigue life of axially loaded specimens was estimated using a base material *S-N* curve obtained in uniaxial testing. In [18] on the other hand, both the base material *S-N* curve and the reduced fatigue tests results were obtained through out-of-plane bending fatigue testing. In this work, the starting curve is obtained through uniaxial testing and the results to be predicted are subjected to an out-of-plane bending state, which imposes an additional challenge. The differences observed in fatigue life between the two loading types (bending and axial) can be attributed to stress gradient and stressed volume effects [29].

One approach to convert HCF *S-N* curves between loading modes is to apply scale factors at 10^3 and 10^6 cycles, where the difference between the load cases typically is larger at 10^3 cycles [30]. In [29] a factor of 1.2 and 1.0–1.1 on the fatigue limit was proposed when going from axially loaded cylindrical specimens to simple/pure bending and rotating bending of cylindrical specimens, respectively. The motivation for having a factor close to 1 when estimating the rotating bending fatigue curve is that the volume subject to high stresses was similar to axially loaded specimens. The specimens subjected to simple bending had on the other hand a smaller process volume and hence a smaller probability of critical defects in the stressed volume.

In this work both the axially loaded specimens and the specimens subject to bending are designed so that the surface area where the crack is expected to initiate is relatively small in both cases, hence the scale factor at 10^6 cycles were assumed to obtain a value of 1.

At 10^3 cycles the stress gradient effect will be more exhibited due to micro-plastic deformation and hence the scale factor is often larger than for lower stresses. Due to the plastic deformation the nominal stress at the surface becomes greater than the true surface stress in bending and hence the bending *S-N* curve deviates from the axially obtained curve. As a rule of thumb, the baseline fatigue strength at 10^3 cycles is proposed in [30] to be $0.9\sigma_{uts}$ in bending and $0.75\sigma_{uts}$ for axial loading. This yields a conversion factor b of 1.2 at $N = 10^3$ going from an axially obtained *S-N* curve to a curve for specimens subject to bending.

In this work the scale factor b^2 is applied at 10^0 cycles to avoid the introduction of an additional exponent. Instead, Eq. (3) can be reused so that the base material *S-N* curve in bending $\sigma_{a-1,b}(N)$ is estimated from the uniaxial curve $\sigma_{a-1}(N)$ by

$$\sigma_{a-1,b} = b^2 \left(\frac{1}{b^2}\right)^{h_t} \sigma_{a-1}, \tag{11}$$

which produces the desired value of $b = 1.2$ at 10^3 cycles. This creates an estimate of the base material *S-N* curve in bending according to the example shown in Fig. 7 if limits are set according to $0 \leq h_t \leq 1$. Hence, for estimation of reduced fatigue life in bending starting from a *S-N* curve obtained from axial testing, it is proposed that the base material *S-N* curve σ_{a-1} in Eqs. (2) and (6) should be replaced by $\sigma_{a-1,b}$ as obtained by Eq. (11).

In the FKM-guideline [31] it is stated the static strength of a non-welded component subject to bending can be scaled using a section factor $n_{pl,b}$, which is calculated by

$$n_{pl,b} = \text{Min}\left(\sqrt{R_{p,max}/\sigma_y}\,;\, f_r K_{p,b}\right), \tag{12}$$

where $R_{p,max}$ is a material group parameter that for elastic stress concentrations lower than three is 1150 MPa for steel, and 400 MPa for wrought aluminum. The hardening factor f_r is calculated by

$$f_r = 0.5\left(1 + \frac{\sigma_{uts}}{\sigma_y}\right), \tag{13}$$

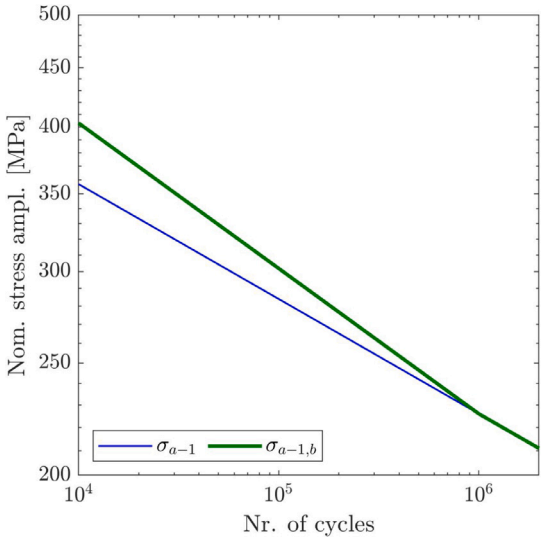

Fig. 7. Example of estimation of base material *S-N* curve in bending $\sigma_{a-1,b}(N)$ using Eq. (11), starting from a curve obtained in uniaxial testing.

Table 5
Residual stresses (XRD measurements) and clamping mean stresses (simulated) in the loading direction of the specimens.

Mtrl.	Residual stress [MPa]	Std. Dev. [MPa]	Clamping mean stress [MPa]
HR CP800SF	300.8	14.7	107
HR CP800SF (SP)	−590.4	25.6	86
HR DP600	222.8	30.1	1
HR DP600 (SP)	−381.5	26.3	−39
HR DP780	297.5	14.5	27
HR DP780 (SP)	−435.9	28.7	−34

and the plastic notch factor $K_{p,b}$ is 1.5 and 1.7 for rectangular cross sections and circular cross sections, respectively. Even though this scale factor was not intended to be used for fatigue life assessment it produces values in the same order of magnitude as the traditional scale factor while distinguishing between material grades and types of material. Hence, it was also examined to replace $b = 1.2$ by $b = n_{pl,b}$.

4. Results

4.1. Residual stress measurements and mean stresses from clamping

The XRD residual stress measurements and the clamping mean stress σ_m obtained from FEM simulations are presented in Table 5. Larger angles after forming (see Table 2) results, as expected, in a higher magnitude of stress. Negative angles result in negative mean stresses and vice versa for positive angles. The magnitudes of the residual stresses seems to correlate with the yield stress, with the highest magnitudes found for the material with the highest yield stress.

4.2. Fatigue life estimation

The fatigue experiment results and the corresponding estimated *S-N* curves are presented in Figs. 8 and 9. The blue lines are the starting curves obtained from uniaxial fatigue testing and red and green curves are the estimations/predictions for formed specimens subject to bending in the critical region. The red curves represent the as formed condition and the green curves the shot-peened condition.

4.3. Crack initiation site

Visible cracks were found in the inner bent radius on samples reaching the fatigue test stopping criterion both at relatively low number of cycles, sometimes below 10^4, and at high number of cycles above 10^6, see Figs. 10–12. This is considered to confirm the validity of the stopping criterion in testing. At one of the inspected samples, shot-peened DP600 with failure at 20 528 cycles no crack was visible by eye, but already in the sample failing at 33 243 cracks were visible.

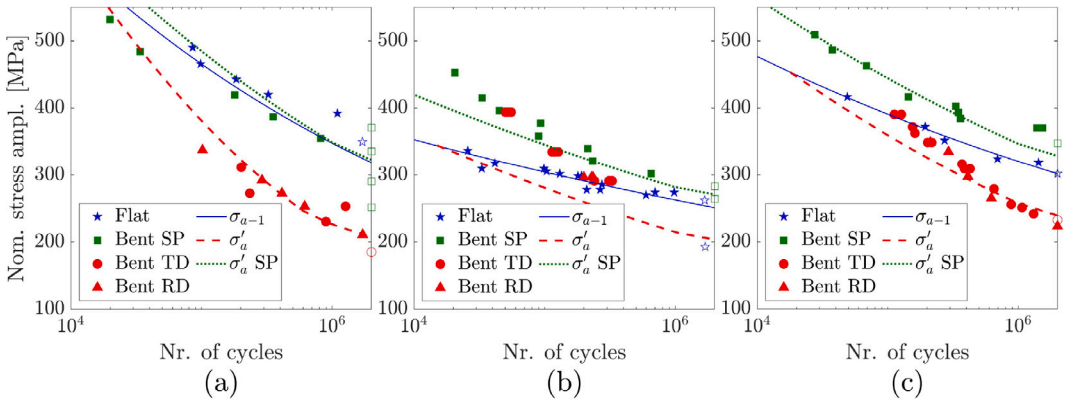

Fig. 8. Fatigue test results and fatigue life estimation using $b = 1.2$ for (a) CP800; (b) DP600; and (c) DP780.

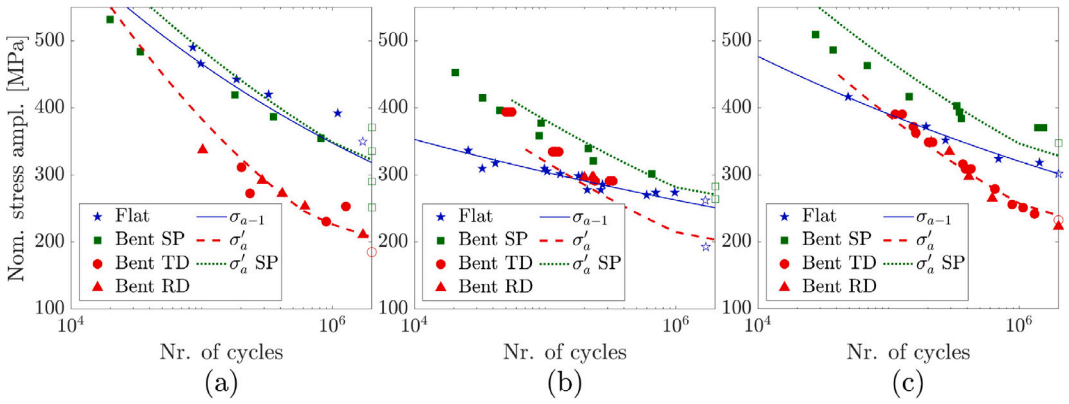

Fig. 9. Fatigue test results and fatigue life estimation using b as calculated by Eq. (12) for (a) CP800; (b) DP600; and (c) DP780.

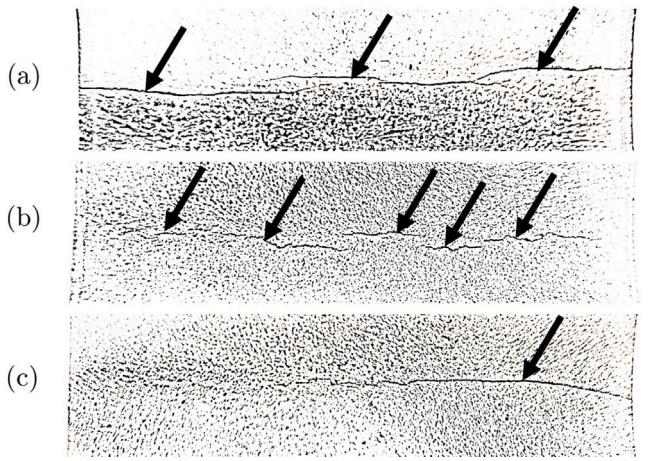

Fig. 10. Examples of fatigue crack formation in inner radius of the bent specimen of CP800 failing at (a) $N = 896\ 633$; (b) $N = 5\ 544$ (shot-peened); and (c) $N = 816\ 797$ (shot-peened).

5. Discussion

5.1. Predicting performance and conversion between nominal S-N curves for different loading modes

As presented in Fig. 13 a scale factor of 1.2 at $N = 10^3$ going from *S-N* curves for uniaxial fatigue to curves for bending seems to yield more conservative, and in terms of predicting performance, worse results than the other proposed method. This is particularly

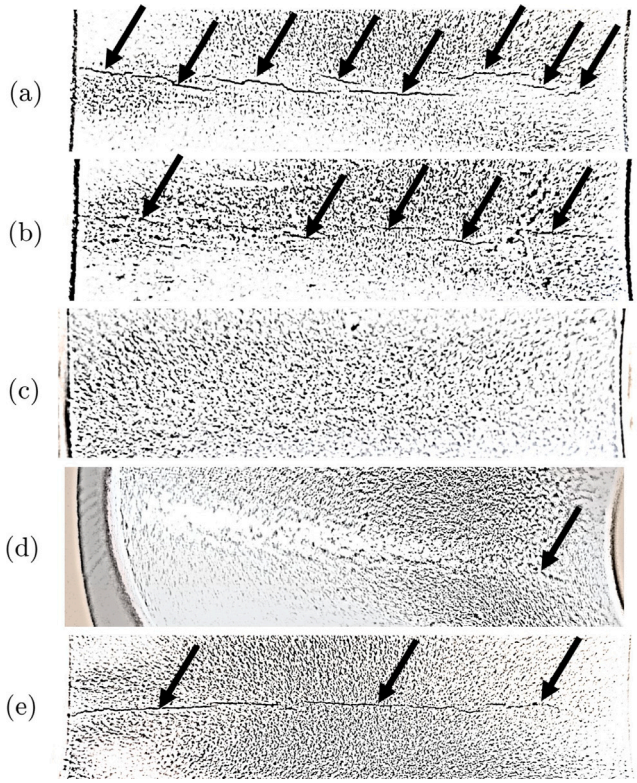

Fig. 11. Examples of fatigue crack formation in inner radius of the bent specimen of DP600 failing at (a) N = 52 527; (b) N = 310 371; (c) N = 20 528 (shot-peened); (d) N = 33 242 (shot-peened); and (e) N = 654 823 (shot-peened).

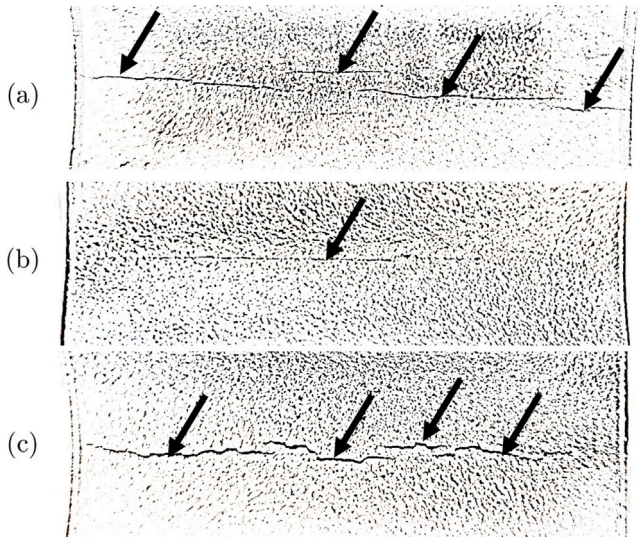

Fig. 12. Examples of fatigue crack formation in inner radius of the bent specimen of DP780 failing at (a) N = 622 217; (b) N = 1 535 892 (shot-peened); and (c) N = 27 645 (shot-peened).

true for the lowest grade steel which also features the lowest yield ratio (σ_y/σ_{uts}). One explanation is likely the stress gradient due to bending which, in some sense, can be treated as a notch. It was shown in [32] that high strength steels with high yield ratio were more sensitive to notches than steels with low yield ratio. For smooth specimens and notch free specimens the fatigue life at a given load increased with increased yield stress. The explanation given for this was that high yield ratio usually indicate cyclic softening and low yield ratio results in cyclic hardening. This means that in cases where the fatigue testing is load controlled and stress

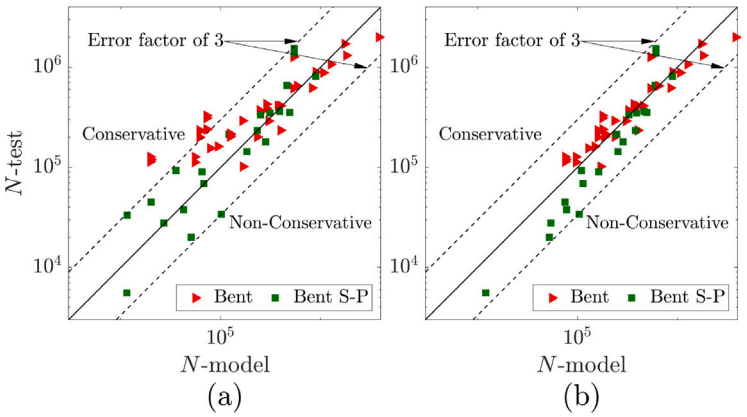

Fig. 13. Predicting performance using (a) $b = 1.2$; and (c) b according to Eq. (12).

gradients exist, the local strain amplitude in the critical area are likely to decrease for materials subject to cyclic hardening [33]. Smaller local strains than assumed mean longer fatigue life than expected. Following this reasoning, the increase in fatigue life is expected to be larger for DP600 with a low yield ratio when going from axial loading to bending. This phenomenon can occur well below the monotonic yield stress in the HCF regime [34]. In fact, the cyclic yield stress and the endurance limit stress at 10^6 cycles are often comparable for metals [35]. However, the yield ratio was not the only factor affecting the ability to handle stress gradients in fatigue as reported in [32]. The yield stress had also an influence. This dual dependency is reflected by the FKM scale factor [31] for static strength assessment presented in Eq. (12). The application of this scale factor in a fatigue framework needs, however, further validation.

5.2. Clamping induced mean stresses

Ignoring the clamping induced residual stresses would have a negative impact on the predicting performance of the model. Especially for CP800 where the stresses are above 100 MPa. In that case neglecting clamping induced stresses causes five of the estimations to end up outside of an error factor of three. Hence it is concluded that rather small deviations of the resulting shape after forming can induce clamping stresses that have an impact on the fatigue life. Knowing this, it is tempting to think that assembly induced residual stresses can be used to increase the fatigue life of components. This could be achieved by designing the forming process for a specific amount of mismatch between two parts, which during the assembly would introduce compressive residual stresses in regions susceptible to fatigue.

5.3. Material sensitivity to forming processes

In Fig. 14 the experiments for all studied materials are plotted in the same graphs with one graph for each condition. They demonstrate that the benefit from choosing the best performing material in straight specimen uniaxial fatigue vanishes after the forming process and especially for lives around 10^6 cycles, something also observed for steels in [17,36] while the aluminum results were significantly lower in [17]. The processes in the referred works were punching and/or trimming rather than stamping. After shot peening the higher strength steels are again distinguished from the lower strength. Interestingly, DP780 end up at approximately the same level as CP800 even though the yield stress is significantly lower. Hence, a hypothesis could be that the HCF performance correlates with yield stress in uniaxial as-rolled condition (in line with previous discussion for smooth specimens [32]). On the other hand, it seems to correlate with material type in stamped condition where high tensile residual stresses are present, and with ultimate tensile strength in shot-peened condition where compressive residual stresses are introduced. One explanation for finding a correlation between fatigue life and tensile strength rather than yield stress for shot-peened specimens might be that the shot peening process introduces severe plastic deformation at the surface increasing the true surface yield stress to values that correlate more with tensile strength than the initial yield stress. It should be noted that the experimental results are obtained at slightly different mean stresses due to the different springback from forming.

5.4. Residual stresses and base material surface condition

The base material in the as-rolled condition was measured to have compressive residual stresses in the magnitude of 100 MPa for the higher strength materials. This was not accounted for in the base material *S-N* curve, in line with previous works [17,18]. This stress level can vary along the rolled sheet and is dependent on the rolling process itself, and on the coiling process, which can cause significant variations in residual stress level on the top and bottom surface of the sheet [37]. The surface roughness after rolling can also vary. To increase the accuracy and robustness of the proposed fatigue life estimation method, it would be valuable

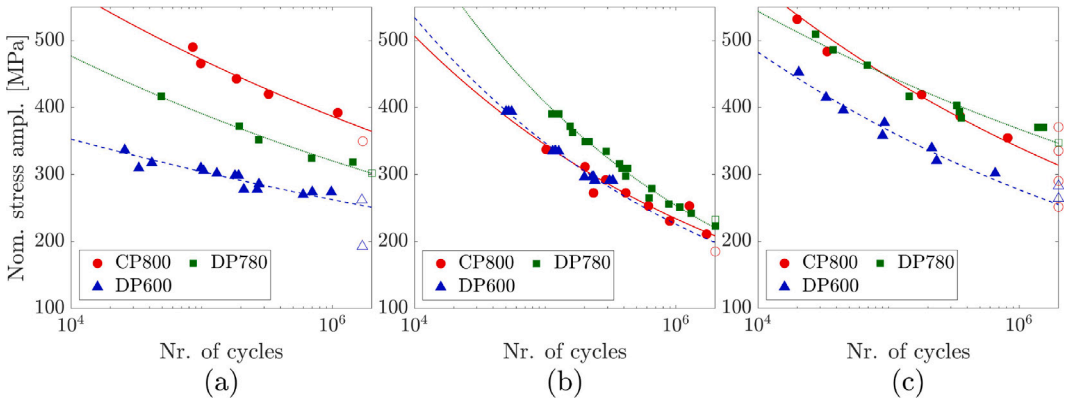

Fig. 14. Fatigue test results from (a) uniaxial fatigue of straight specimens with polished edges; (b) Fatigue of bent specimens; and (c) fatigue of bent specimens after shot peening. Curves are fitted to the experiments for illustration.

in the future to specify for which range of initial surface roughness and residual stress (for the as-rolled surface condition) this estimation approach is valid. Another possibility could be to develop a methodology to adjust the initial base material *S-N* curve based on the true as-rolled surface condition. This could require adjustment of for example the residual stress relaxation criterion to achieve satisfactory life estimation predictions.

The residual stress relaxation model is implemented using the nominal maximum stress level including mean stress from loading but before mean stress correction including the relaxed residual stress. This means that the stress relaxation is calculated based on a nominal stress level and not at the actual stress level at testing, an approach that has proven capabilities in fatigue life estimation [17,18]. However, the relaxation model and stress relaxation behavior of formed and shot-peened specimens should be studied more in detail to increase the understanding and to build confidence in the phenomenological relaxation model implementation.

Preliminary studies using a Morrow mean stress correction model and calculating the relaxation based on the reduced stress, or the actual stress at the reduced load level, show promising results. However, this requires a reduction of the tensile stress relaxation threshold from the monotonic yield strength to, approximately, the cyclic yield strength. The Morrow criterion is similar to the Goodman criterion but uses the true fracture strength instead of the ultimate tensile strength. For steels, this value can often be estimated by adding 345 MPa to σ_{uts} [38].

5.5. Geometrical aspects from forming

In this work the geometry after forming was measured along the center line of the specimens as presented in Fig. 3. It was assumed in the FEM simulations and in the nominal stress calculation that the cross section was rectangular and that the nominal sheet thickness was applicable. In fact some thinning is expected to occur in the radius and the edges of the cross section in the bent radius turns upwards slightly. To capture this, more extensive geometrical measurement, or an accurate forming simulation should be performed.

5.6. Effect of rolling direction

As presented in Figs. 8 and 9 formed specimens cut both in the transverse to rolling and in the rolling direction were tested. No significant differences in fatigue life or in the measured residual stresses were found between the two groups.

5.7. Possibility of using FEM forming simulations instead of residual stress measurements

Forming simulations are sometimes more convenient than experimental measurements of residual stresses. To explore the possibilities of using simulations instead of measurements a simple forming simulation of CP800 using the material parameters calibrated in [23] was performed. Fully integrated 3D shell elements were used. As presented in Fig. 15 a similar shape as the measured formed part, created from center-line measurements according to Fig. 3, was achieved.

The residual stress value in the loading direction, measured in the center of the inner radius was 301 MPa (approx. $0.4\sigma_y$) according to the XRD measurements, as compared to 438 MPa (approx. $0.6\sigma_y$) obtained from simulations. The main reason for this is probably the simplified simulation setup using 3D shell elements. In [39], residual stress predictions in cold-formed steel sections using 3D solid elements and 3D shell elements were compared. It was shown that the predicted transversal (corresponding to the loading direction in this work) tensile residual stresses at the formed radius inner surface, were clearly higher in the simulations using 3D shells as compared to 3D solids. More work on the simulation setup and probably also the material model would be

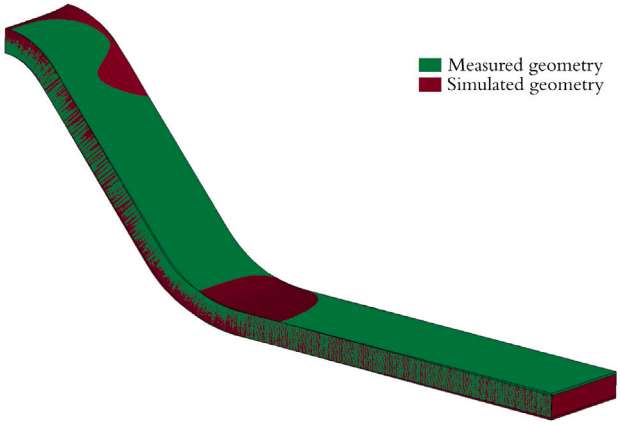

Fig. 15. Comparison of simulated and measured bent specimen geometry after forming (one quarter of the specimen). The simulated geometry is created by displaying the shell thickness.

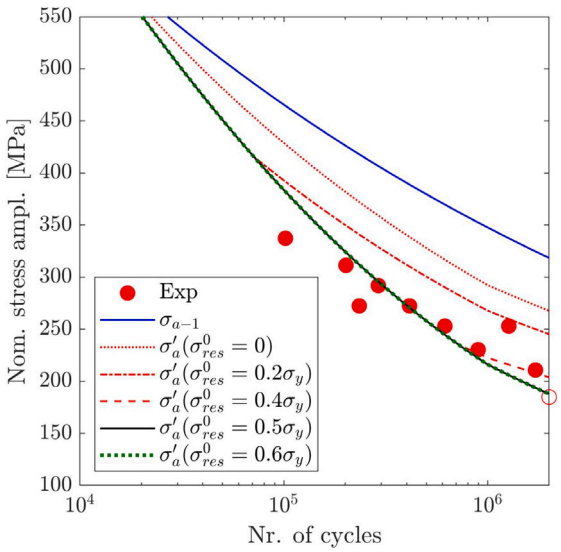

Fig. 16. Estimation of reduced fatigue *S-N* curves using different initial residual stresses σ^0_{res} from forming.

necessary to decrease the difference between simulations and measurements. However, this was considered out of scope for this work.

To explore the effect of the discrepancy in residual stress as obtained from FEM and XRD, the initial residual stress given to the life estimation model was varied. The results are presented in Fig. 16. Above a certain stress level around $0.4\sigma_y$ the effect of further increasing the residual stress level at 10^6 cycles is a few percent on the stress amplitude, according to the model. Around $0.5\sigma_y$ the effect of increasing the initial residual stress vanishes completely. This implies that in cases where high residual stresses are found, which is often the case in forming, the accuracy of the residual stress estimation obtained from FEM is not crucial for the applicability of the life estimation approach presented here. If residual stresses below this threshold (0.4-0.5σ_y) is expected, then more accurate simulations could provide beneficial insights to for example process parameter effect on fatigue life. This hypothesis requires however further validation.

6. Conclusions

In this work, fatigue of formed and shot-peened specimens of high strength steels subjected to a bending stress state was studied. A fatigue life estimation procedure was proposed, starting from a base material *S-N* curve obtained from uniaxial fatigue testing. The method requires no parameter fitting and relies solely on static tensile properties.

The main conclusions from this study are:

1. Considering the yield ratio and yield stress can improve conversion between *S-N* curves for uniaxial loading and *S-N* curves for bending.
2. For polished edges, the yield stress is a good indicator of relative fatigue strength, whereas for formed areas, selecting a steel with increased yield strength does not increase the expected HCF life.
3. The results indicate that, for shot-peened components, tensile strength may be a better indicator of fatigue performance than yield strength.
4. Utilization of appropriate post-processes, such as shot peening, in formed areas is crucial to benefit from increased steel grades in terms of HCF performance and weight saving potential.
5. The model suggests that reducing initial residual stresses does not significantly increase fatigue life if not reduced below a level of ($\sim 0.5\sigma_y$). This suggestion requires further validation.
6. Clamping or assembly stresses should be considered in the design of components susceptible to fatigue.

CRediT authorship contribution statement

David Gustafsson: Writing – original draft, Validation, Software, Methodology, Investigation, Formal analysis, Conceptualization. **Davide Ronco:** Writing – review & editing, Resources, Investigation, Conceptualization. **Giorgio Gallio:** Writing – review & editing, Resources, Investigation, Funding acquisition, Conceptualization. **Erik Olsson:** Writing – review & editing, Supervision, Project administration, Funding acquisition, Conceptualization.

Declaration of competing interest

The authors declare that they have no known competing financial interests or personal relationships that could have appeared to influence the work reported in this paper.

Acknowledgments

The authors would like to thank the European Union for providing funding of the Steel4Fatigue project (Research Fund for Coal and Steel (RFCS): project no. 101157245) and the Fatigue4Light project (Horizon 2020, LC-GV-06-2020 project no. 101006844) in which this study was conducted.

Appendix. Fatigue test results

See Tables A.1–A.3.

Data availability

Data will be made available on request.

Table A.1
Fatigue test results of flat specimens with polished edges made from HR CP800SF (nom. t = 3.7 mm), HR DP600 (nom. t = 3.5 mm), and HR DP780 (nom. t = 3.0 mm).

Mtrl.	Amp. F_y [N]	N [cycles]
CP800	25 700	324 677
CP800	30 000	85 501
CP800	24 000	1098193
CP800	27 100	184 666
CP800	28 500	98 472
CP800	21 400	> 1706285
DP600	17 250	980 910
DP600	19 000	130 592
DP600	19 250	103 453
DP600	17 500	209 975
DP600	18 000	274 343
DP600	17 250	700 714
DP600	19 500	98 706
DP600	20 000	41 542
DP600	17 500	266 134
DP600	19 500	33 013
DP600	17 000	596 924
DP600	21 200	25 782
DP600	18 800	179 703
DP600	18 800	191 527
DP600	12 135	> 1693744
DP600	16 500	> 1679676
DP780	19 000	272 938
DP780	20 100	193 844
DP780	22 500	49 020
DP780	17 500	694 216
DP780	17 200	1430924
DP780	16 300	> 2000000

Table A.2
Fatigue test results of bent specimens made from HR CP800SF (nom. t = 3.7 mm), HR DP600 (nom. t = 3.5 mm), and HR DP780 (nom. t = 3.0 mm).

Mtrl.	Amp. F_y [N]	N [cycles]
CP800	780	615 956
CP800	900	290 502
CP800	840	413 167
CP800	650	1713858
CP800	840	234 202
CP800	780	1267633
CP800	710	896 633
CP800	960	201 514
CP800	1040	101 733
CP800	570	> 2000000
DP600	1037	50 190
DP600	766	310 371
DP600	881	120 310
DP600	766	240 583
DP600	881	127 044
DP600	766	328 822
DP600	881	114 056
DP600	881	118 723
DP600	881	120 025
DP600	1037	55 418
DP600	1037	52 527
DP600	780	228 534
DP600	780	199 593
DP600	766	238 457
DP600	780	234 540
DP780	680	370 838
DP780	780	161 717
DP780	840	112 473
DP780	600	652 193
DP780	540	1070423
DP780	720	292 327
DP780	640	411 986
DP780	480	> 2000000
DP780	750	212 049
DP780	570	622 217
DP780	665	427 585
DP780	665	387 652
DP780	750	217 003
DP780	800	154 999
DP780	840	127 128
DP780	750	202 430
DP780	550	883 325
DP780	520	1311468
DP780	500	> 2000000

Table A.3
Fatigue test results of bent and shot-peened specimens made from HR CP800SF (nom. t = 3.7 mm), HR DP600 (nom. t = 3.5 mm), and HR DP780 (nom. t = 3.0 mm).

Mtrl.	Amp. F_y [N]	N [cycles]
CP800	780	> 2000000
CP800	900	> 2000000
CP800	1040	> 2000000
CP800	1100	816 797
CP800	1150	> 2000000
CP800	2000	5544
CP800	1300	179 260
CP800	1650	19 956
CP800	1500	33 901
CP800	1200	353 073
DP600	1200	20 528
DP600	1000	93 126
DP600	800	654 823
DP600	900	214 052
DP600	1100	33 243
DP600	1050	45 057
DP600	950	89 985
DP600	850	233 268
DP600	750	> 2000000
DP600	700	> 2000000
DP780	1000	68 828
DP780	900	143 968
DP780	1100	27 645
DP780	800	1388625
DP780	850	348 666
DP780	1050	37 685
DP780	830	360 607
DP780	870	332 893
DP780	800	1535892
DP780	750	> 2000000

References

[1] S.K. Paul, Effect of forming strain on low cycle, high cycle and notch fatigue performance of automotive grade dual phase steels: A review, Forces Mech. 11 (2023) 100184, http://dx.doi.org/10.1016/J.FINMEC.2023.100184.

[2] D. Shang, X. Liu, Y. Shan, E. Jiang, Research on the stamping residual stress of steel wheel disc and its effect on the fatigue life of wheel, Int. J. Fatigue 93 (2016) 173–183, http://dx.doi.org/10.1016/J.IJFATIGUE.2016.08.020.

[3] G. Leister, Passenger car tires and wheels:, Dev. - Manuf. - Appl. Passeng. Car Tires Wheel.: Dev. - Manuf. - Appl. (2018) 1–273, http://dx.doi.org/10.1007/978-3-319-50118-5.

[4] Q. Jiang, Z. Zhao, Z. Xu, J. Sun, X. Chen, B. Su, Z. Zhao, W. Jiang, Effect of residual stresses on wheel fatigue life and experimental validation, Mach. 2022 10 (2022) 924 10, http://dx.doi.org/10.3390/MACHINES10100924, 924.

[5] G. Marcuccio, E. Bonisoli, S. Tornincasa, J.E. Mottershead, E. Patelli, W. Wang, Image decomposition and uncertainty quantification for the assessment of manufacturing tolerances in stress analysis, J. Strain Anal. Eng. Des. 49 (2014) 618–631, http://dx.doi.org/10.1177/0309324714533694.

[6] J. Meng, P. Zhu, Z. Liu, Q. Ji, Integration of multi-step stamping effects in the bending fatigue analysis of a steel wheel, Fatigue Fract. Eng. Mater. Struct. 36 (2013) 795–808, http://dx.doi.org/10.1111/FFE.12047.

[7] M.L. Facchinetti, B. Weber, C. Doudard, S. Calloch, Coupling of forming process and fatigue design computations: A local approach, Adv. Eng. Mater. 11 (2009) 736–741, http://dx.doi.org/10.1002/ADEM.200900041.

[8] J. Kašpar, P. Bernardin, V. Lašová, Fatigue estimation using inverse stamping, Met. 2023 13 (2023) 1956 13, http://dx.doi.org/10.3390/MET13121956, 1956.

[9] P.J. McGrath, D.G. Hattingh, M.N. James, A. Els-Botes, Effects of forming process on fatigue performance of wheel centre discs, in: ECF13, San Sebastian, 2000, p. 2013.

[10] S. Venturini, C. Rosso, M. Velardocchia, An automotive steel wheel digital twin for failure identification under accelerated fatigue tests, Eng. Fail. Anal. 158 (2024) 107979, http://dx.doi.org/10.1016/J.ENGFAILANAL.2024.107979.

[11] D. Löhe, J.E. Hoffmann, Influence of macro residual stresses on the fatigue behavior smooth and notched specimens made from a high strength steel, SAE Trans. 111 (2002) 704–710.

[12] J. Hensel, Mean stress correction in fatigue design under consideration of welding residual stress, Weld. the World 64 (2020) 535–544, http://dx.doi.org/10.1007/S40194-020-00852-Z.

[13] T. Pertoll, C. Buzzi, M. Leitner, L. Boronkai, Application of local fatigue strength approach to assess and optimise the impact of deep rolling on the fatigue performance of railway axles, Int. J. Fatigue 185 (2024) 108335, http://dx.doi.org/10.1016/J.IJFATIGUE.2024.108335.

[14] P. Ghosal, S.K. Paul, A. Raj, Influence of uniaxial and biaxial pre-straining on the high cycle fatigue performance of dp590 steel, Int. J. Fatigue 151 (2021) 106369, http://dx.doi.org/10.1016/J.IJFATIGUE.2021.106369.

[15] X. Wang, X. Zhang, Simulation of dynamic cornering fatigue test of a steel passenger car wheel, Int. J. Fatigue 32 (2010) 434–442, http://dx.doi.org/10.1016/J.IJFATIGUE.2009.09.006.

[16] S. Gothivarekar, S. Coppieters, R. Talemi, D. Debruyne, Effect of bending process on the fatigue behaviour of high strength steel, J. Constr. Steel Res. 182 (2021) 106662, http://dx.doi.org/10.1016/J.JCSR.2021.106662.

[17] D. Gustafsson, S. Parareda, R. Munier, E. Olsson, High cycle fatigue life estimation of punched and trimmed specimens considering residual stresses and surface roughness, Int. J. Fatigue 186 (2024) 108384, http://dx.doi.org/10.1016/J.IJFATIGUE.2024.108384.

[18] D. Gustafsson, S. Parareda, H. Sieurin, E. Olsson, Estimating the effect of punching on out-of-plane bending fatigue of steel sheet specimens, Eng. Fail. Anal. 173 (2025) 109415, http://dx.doi.org/10.1016/J.ENGFAILANAL.2025.109415.

[19] H. Gerber, Bestimmung der zulässigen spannungen in eisen-constructionen, Z. Des Bayer. Arch. Und Ingenieur-Vereins 6 (1874) 101–110.

[20] J. Goodman, Mechanics Applied To Engineering, Green & Company, Longmans, 1899.

[21] A. Niesł ony, M. Böhm, Mean stress effect correction using constant stress ratio s–n curves, Int. J. Fatigue 52 (2013) 49–56, http://dx.doi.org/10.1016/J.IJFATIGUE.2013.02.019.

[22] B. Das, S.K. Paul, A. Singh, K.S. Arora, M. Shome, The effect of thickness variation and pre-strain on the cornering fatigue life prediction of a dp600 steel wheel disc, Int. J. Fatigue 139 (2020) 105799, http://dx.doi.org/10.1016/J.IJFATIGUE.2020.105799.

[23] D. Gustafsson, S. Parareda, L. Ortiz-Membrado, A. Mateo, E. Jiménez-Piqué, E. Olsson, Simulation of metal punching and trimming using minimal experimental characterization, J. Mater. Process. Technol. 321 (2023) 118148, http://dx.doi.org/10.1016/J.JMATPROTEC.2023.118148.

[24] M. Rout, S.K. Pal, S.B. Singh, Finite Element Modeling of Hot Rolling: Steady- and Unsteady-State Analyses, Woodhead Publishing, 2017, pp. 83–124, http://dx.doi.org/10.1016/B978-0-85709-481-0.00004-5.

[25] S. Lee, S.J. Kim, The effect of thickness of the hot-rolled sheet on the magnetic properties of non-oriented electrical steel, J. Magn. Magn. Mater. 599 (2024) 172086, http://dx.doi.org/10.1016/J.JMMM.2024.172086.

[26] X. Li, X. Zhou, Q. Jiang, Z. Liu, The prediction of the mechanical properties for hot-rolled nb micro-alloyed dual-phase steel based on microstructure characteristics, JOM 75 (2023) 2225–2234, http://dx.doi.org/10.1007/S11837-023-05795-6.

[27] P. Magnetto, G. Gotta, F. R. D, D. Pieronek, P. Tlauka, Method for the mechanical characterization of a metallic material for wheel disk production, Eur. Pat. Off. EP3115767 (2015).

[28] O.H. Basquin, The exponential law of endurance tests, in: Proc. Annual Meeting, American Society for Testing Materials, vol. 1910, pp. 625–630.

[29] P.P. Milella, Fatigue and Corrosion in Metals, second ed., Springer-Verlag Wien, 2013, http://dx.doi.org/10.1007/978-3-031-51350-3.

[30] Y.L. Lee, J. Pan, R.B. Hathaway, M.E. Barkey, Fatigue Testing and Analysis: Theory and Practice, first ed., Elsevier, 2004, http://dx.doi.org/10.1016/B978-0-7506-7719-6.X5000-3.

[31] R. Rennert, E. Kullig, A. Esderts, M. Vormwald, M. Luke, FKM-Guideline: Analytical Strength Assessment, English Version, Seventh ed., VDMA-Verlag, 2020.

[32] J.O. Sperle, Fatigue strength of high strength dual-phase steel sheet, Int. J. Fatigue 7 (1985) 79–86, http://dx.doi.org/10.1016/0142-1123(85)90037-4.

[33] Z. Zhang, Cyclic Hardening/Softening, Springer US, 2013, pp. 687–691, http://dx.doi.org/10.1007/978-0-387-92897-5_245.

[34] S.K. Paul, A review on cyclic hardening and softening behavior of alloys, J. Alloy. Met. Syst. 9 (2025) 100153, http://dx.doi.org/10.1016/J.JALMES.2025.100153.

[35] S.K. Paul, Correlation between endurance limit and cyclic yield stress determined from low cycle fatigue test, Materialia 11 (2020) 100695, http://dx.doi.org/10.1016/J.MTLA.2020.100695.

[36] N. Heshmati, M. Hoseini-Athar, E. Olsson, A. Borgenstam, H. Sieurin, J. Larsson, T.L. Lee, P. Hedström, On the overlooked role of microstructure to explain post-punching fatigue performance of advanced high-strength steel, Mater. Sci. Eng.: A 927 (2025) 147946, http://dx.doi.org/10.1016/J.MSEA.2025.147946.

[37] A. Milenin, R. Kuziak, M. Lech-Grega, A. Chochorowski, S. Witek, M. Pietrzyk, Numerical modeling and experimental identification of residual stresses in hot-rolled strips, Arch. Civ. Mech. Eng. 16 (2016) 125–134, http://dx.doi.org/10.1016/J.ACME.2015.08.002.

[38] N.E. Dowling, C.A. Calhoun, A. Arcari, Mean stress effects in stress-life fatigue and the walker equation, Fatigue Fract. Eng. Mater. Struct. 32 (2009) 163–179, http://dx.doi.org/10.1111/j.1460-2695.2008.01322.x.

[39] A. Mutafi, J.M. Irwan, N. Yidris, A.M. Ghaleb, S. Al-Alimi, M. Amran, M. Qasem, M. Hasan, A. Al-Fakih, An in-depth comparative fea on through-thickness residual stresses in press-braked cold-formed steel section, Results Eng. 22 (2024) 102124, http://dx.doi.org/10.1016/J.RINENG.2024.102124.